Electronic Supplementary Material (ESI) for Journal of Materials Chemistry A.

Targeted Capture and Pressure/Temperature-Responsive Separation in Flexible Metal–Organic Frameworks

Libo Li, Yong Wang, Jiangfeng Yang, Xiaoqing Wang, and Jinping Li*

Research Institute of Special Chemicals, Taiyuan University of Technology, Taiyuan 030024, Shanxi, P. R. China
Email: jpli211@hotmail.com

Contents

1. Pelleting process of $[Cu(dhbc)_2(4,4'\text{-bipy})]$ and $[Cu(4,4'\text{-bipy})_2(BF_4)_2]$ Particles

$[Cu(dhbc)_2(4,4'\text{-bipy})]$(Particles 1) - Particles with diameters of 200–300 µm (Figure S1) were obtained by pressing $[Cu(dhbc)_2(4,4'\text{-bipy})]$ powder (at 3 MPa) into a solid disk, keeping pressure for 2 min, and then crushing and sieving to obtain particles of a certain size.

$[Cu(4,4'\text{-bipy})_2(BF_4)_2]$(Particles 2) - Particles with diameters of 220–320 µm (Figure S1) were obtained by pressing $[Cu(4,4'\text{-bipy})_2(BF_4)_2]$ powder (at 3 MPa) into a solid disk, keeping pressure for 2 min, and then crushing and sieving to obtain particles of a certain size.

Finally, the particles were activated by flushing the adsorption bed with helium gas for 2 h at 373 K, and allowed to cool to ambient temperature.

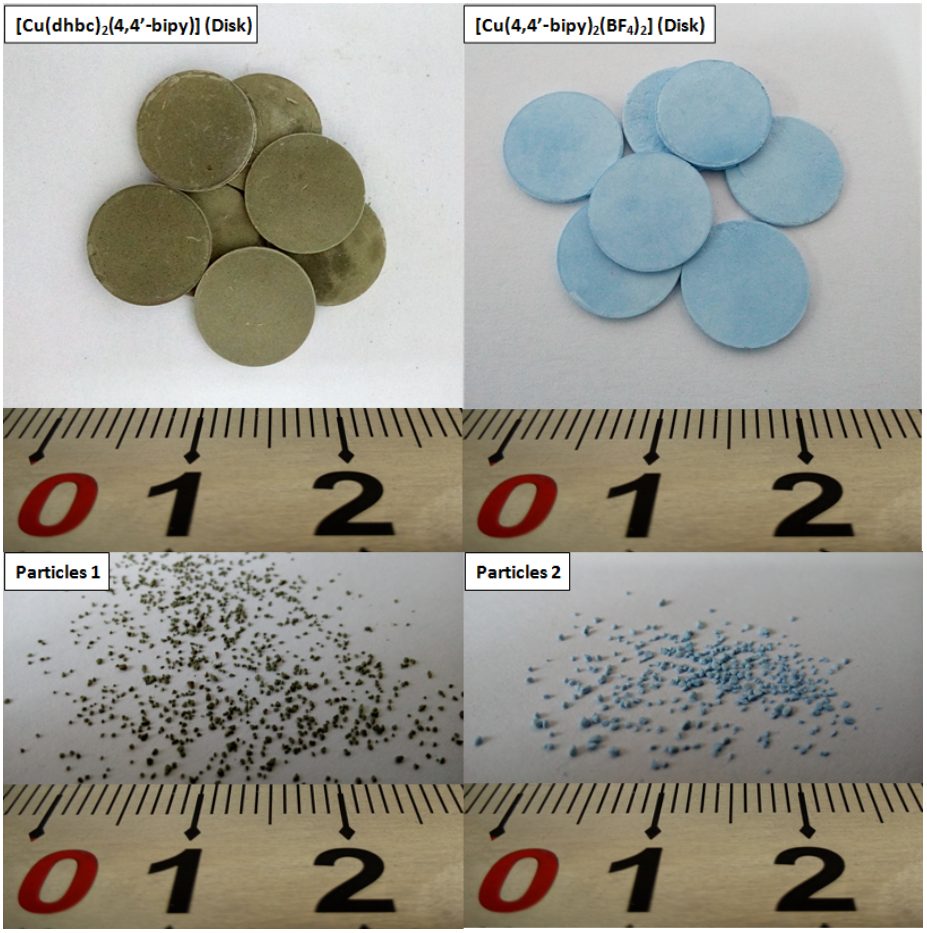

Figure S1. Pelleting process of $[Cu(dhbc)_2(4,4'\text{-bipy})]$ (deep green) and $[Cu(4,4'\text{-bipy})_2(BF_4)_2]$ (blue) Particles.

2. Mechanical stability and gas adsorption abilities of the two particles

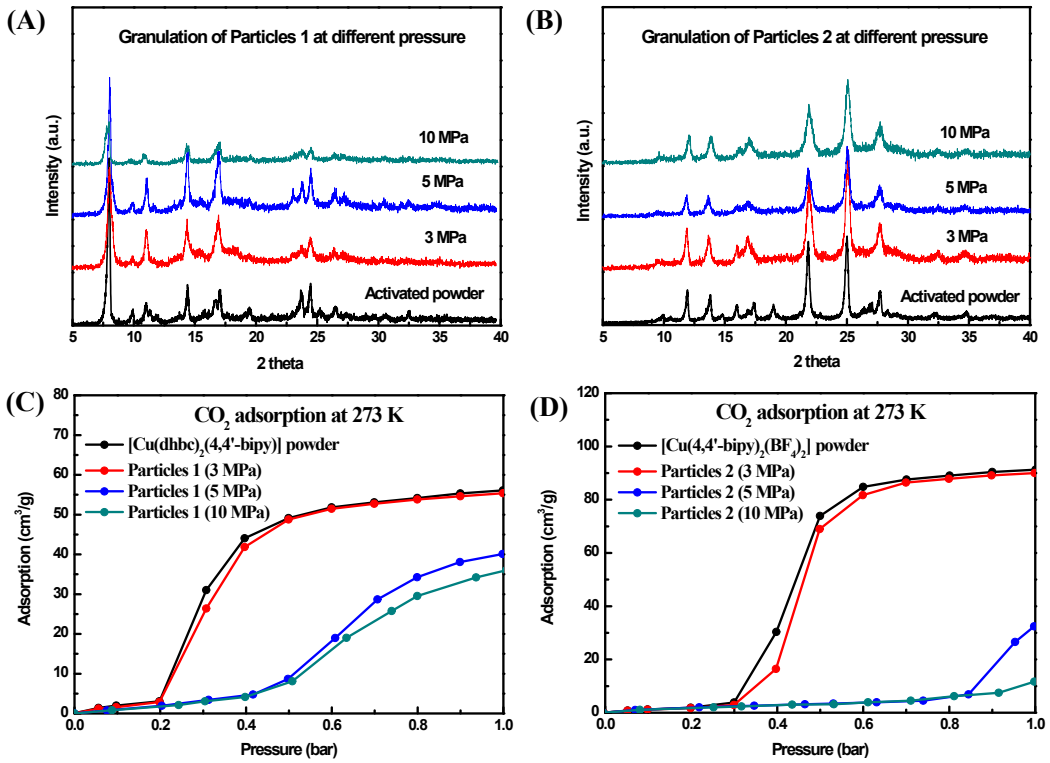

Figure S2. Mechanical stability of particles 1 and 2 at different pelleting pressure were tested by powder X-ray diffraction and CO_2 adsorption at 1 bar and 273 K.

3. The simulation details of Monte Carlo molecular dynamic simulation

Force fields

The potential parameters and partial charges for all of the adsorbates are shown in Table 1. CO_2 was modeled as a linear molecule with three charged LJ interaction sites, one on each atom, with C−O bond length *l* = 1.149 Å, taken from the EPM2 force field developed by Harris and Yung.[1] CH_4 was modeled as a single LJ interaction site, and the potential parameters were taken from the TraPPE force field reported by Potoff and Siepmann.[2] N_2 was also represented using the TraPPE force field, with two of the three charged sites located on the respective N atoms and the third one situated at the center of mass (COM). The N–N bond length was 1.10 Å and only the N atoms were considered as LJ interacting sites.

Table 1 LJ potential and coulombic potential parameters for the adsorbates.

Adsorbate	Site	LJ parameters		
		σ(Å)	ε/k_b (K)	charge (e)
CO_2	CO_2_O	3.033	80.507	-0.3256
	CO_2_C	2.757	28.129	0.6512
CH_4	CH_4	3.73	148.0	0.0
N_2	N_2_N	3.31	36.0	-0.482
	N_2_M	0	0	0.964

The MOF material studied here was modeled by the atomistic representation. The LJ potential parameters for the framework atoms of the MOFs were taken from the Dreiding force field,[3] and the missing parameters for Cu were taken from the universal force field (UFF),[4] as given in Table 2. In this work, atomic partial charges for the frameworks of the MOFs were estimated using the CBAC method developed by Zhong's group, with slight variation to make the total charge equal to zero.[5,6]

Table 2 LJ Potential Parameters for the Atoms in the Framework.

LJ parameters	Cu[a]	C	O	H	N	F	B
σ(Å)	3.11	3.47	3.03	2.85	3.26	3.09	3.58
ε/k_b (K)	2.516	47.86	48.16	7.65	38.95	36.48	47.81

[a)] Taken from the UFF force field (it is missed in the Dreiding force field).

Simulation details

Grand canonical Monte Carlo (GCMC) simulation was performed to calculate the adsorption of the CO_2/CH_4 and N_2/CH_4 mixtures in the MOFs. The Peng–Robinson equation of state was used to convert the pressure into the corresponding fugacity used in the GCMC simulations. For [Cu(dhbc)$_2$(4,4'-bipy)], an expanded 4×3×2

conventional cell with periodic boundary conditions was used as the simulation cell, whereas that for [Cu(4,4'-bipy)$_2$(BF_4)$_2$] was 2×3×3. The cut-off radius was set at 12.8 Å for LJ interactions, and the long-range electrostatic interactions were handled using the Ewald summation technique with tinfoil boundary condition. For each state point, GCMC simulations consisted of 2×10^7 steps to ensure equilibration, followed by 2×10^7 steps to sample the desired thermodynamic properties.

References

1. J. G. Harris, K. H. Yung, *J. Phys. Chem.* 1995, **99**, 12021-12024.

2. J. J. Potoff, J. I. Siepmann, AICHE J. 2001, **47**, 1676-1682.

3. S. L. Mayo, B. D. Olafson and W. A. Goddard, *J. Phys. Chem.* 1990, **94**, 8897-8909.

4. A. K. Rappe, C. J. Casewit, K. S. Colwell, W. A. Goddard and W. M. Skiff, *J. Am. Chem. Soc.* 1992, **114**, 10024-10035.

5. Q. Xu, C. Zhong, *J. Phys. Chem.* C. 2010, **114**, 5035-5042.

6. C. Zheng, C. Zhong, *J. Phys. Chem.* C. 2010, **114**, 9945-9951.

4. CO_2, CH_4, and N_2 adsorption on two particles

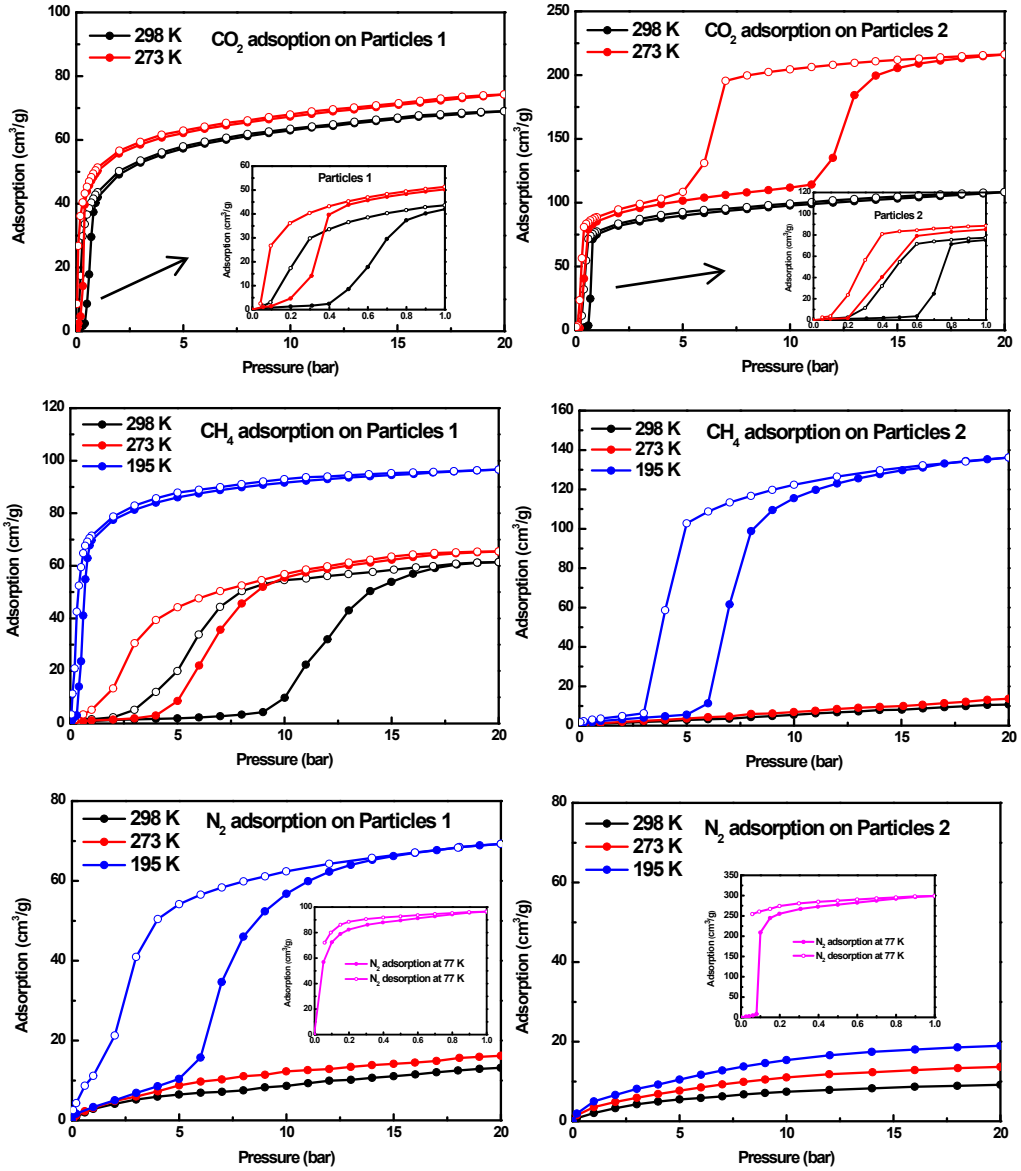

Figure S3. Equilibrium CO_2, CH_4, and N_2 adsorption (filled) and desorption (opened) isotherms of particles 1 (left) and particles 2 (right) at 298 K, 273 K, 195 K and 77 K.

5. Analysis of transient CO_2/CH_4 and CH_4/N_2 breakthrough experiments (Rajamani Krishna)

- Van 't Hoff Institute for Molecular Sciences, University of Amsterdam, Science Park 904, 1098 XH Amsterdam, The Netherlands. Email: r.krishna@contact.uva.nl

(1) We analyze the experimental breakthroughs for separations of CO_2/CH_4 mixtures in packed bed with $[Cu(dhbc)_2(4,4'\text{-bipy})]$ (particles 1) and $Cu(4,4'\text{-bipy})_2(BF_4)_2$ (particles 2).

Figure S4 compares the experimental breakthroughs for CO_2/CH_4 (50%/50%) mixtures with the two MOFs at flow rates of 20 mL min^{-1} and total pressures of 1 bar, 10 bar, and 20 bar, operating at 273 K, and 298 K.

The y-axis represents the mole fraction of CH_4 in the exit gas phase. In each case, it is possible to produce CH_4 with say 99% purity during the time interval between t_1, and t_2. This is illustrated for $[Cu(dhbc)_2(4,4'\text{-bipy})]$ (particles 1) at 20 bar in Figure S4.

A material balance for the time interval $t = t_1 - t_2$ allows us to determine the productivity of CH_4 with the specified 99%+ purity

$$CH_4\ productivity\ = \frac{c_t Q_t}{m_{ads}} \int_{t_1}^{t_2} (y_{CH4,exit}) dt \quad (1)$$

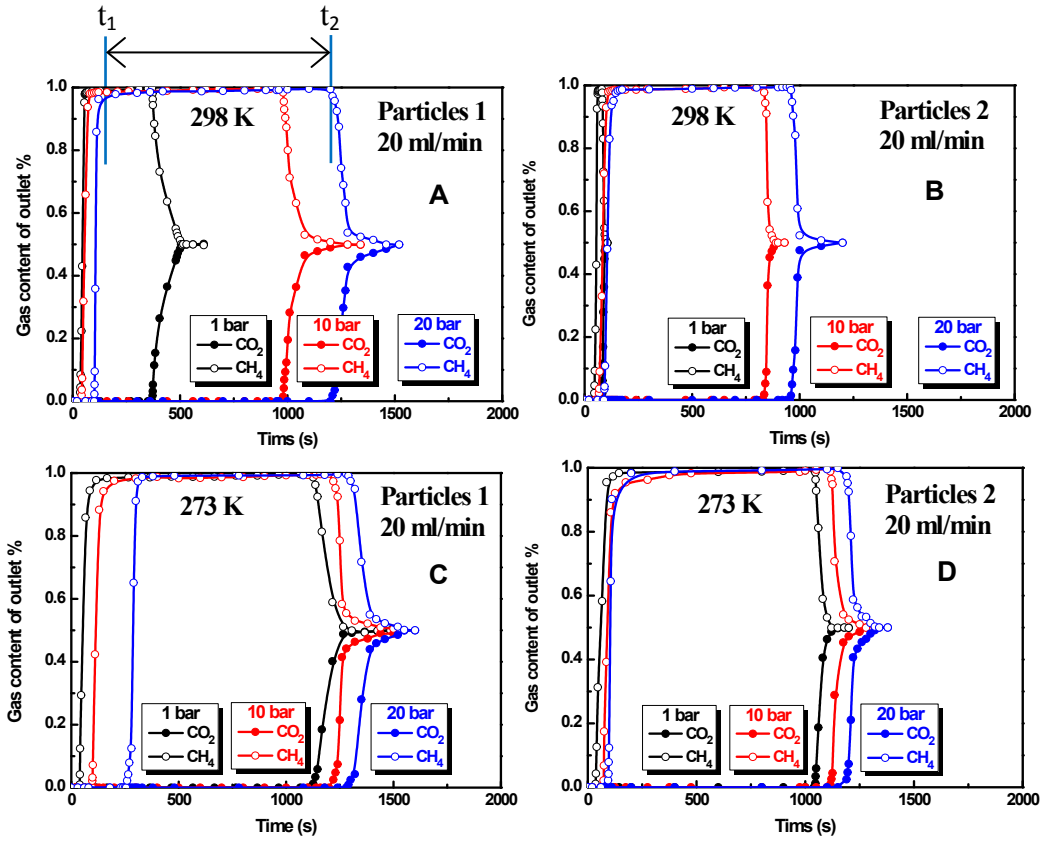

Figure S4. Experimental breakthroughs for 50/50 CO_2/CH_4 mixtures in packed bed with $[Cu(dhbc)_2(4,4'\text{-bipy})]$ (particles 1) and $Cu(4,4'\text{-bipy})_2(BF_4)_2$ (particles 2). The y-axis represents the mole fractions of CO_2 and CH_4 in the

exit gas phase. The inlet gas is equimolar, at total pressures of 1 bar, 10, and 20 bar. As indicated for particles 1 at 298 K and 20 bar, it is possible to produce CH_4 with 99% purity during the time interval between t_1, and t_2.

Figures S5a, and S5b present comparisons of the productivities of 99%+ pure CH_4 for CO_2/CH_4 mixture breakthroughs at 273 K, and 298 K in the two MOFs. The x-axis is the total pressure.

The CO_2 uptake is calculated from a material balance during the time interval 0 – t_{final}, where t_{final} is the final equilibration time.

$$CO_2\ uptake = \frac{c_t Q_t}{m_{ads}} \int_0^{t_{final}} (y_{CO2,exit} - y_{CO2,exit}) dt \quad (2)$$

Figures S6a, S6b are plots of CO_2 captured per kg of MOF as a function of the total pressure.

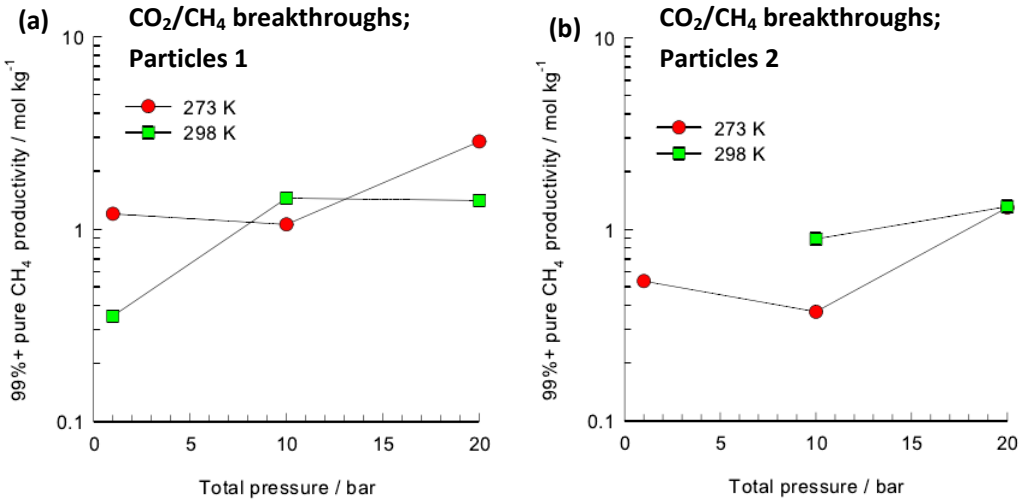

Figure S5. (a, b) Productivity of 99%+ pure CH_4 for CO_2/CH_4 mixture breakthroughs with two particles at 273 K, and 298 K. The x-axis is the total operating pressure.

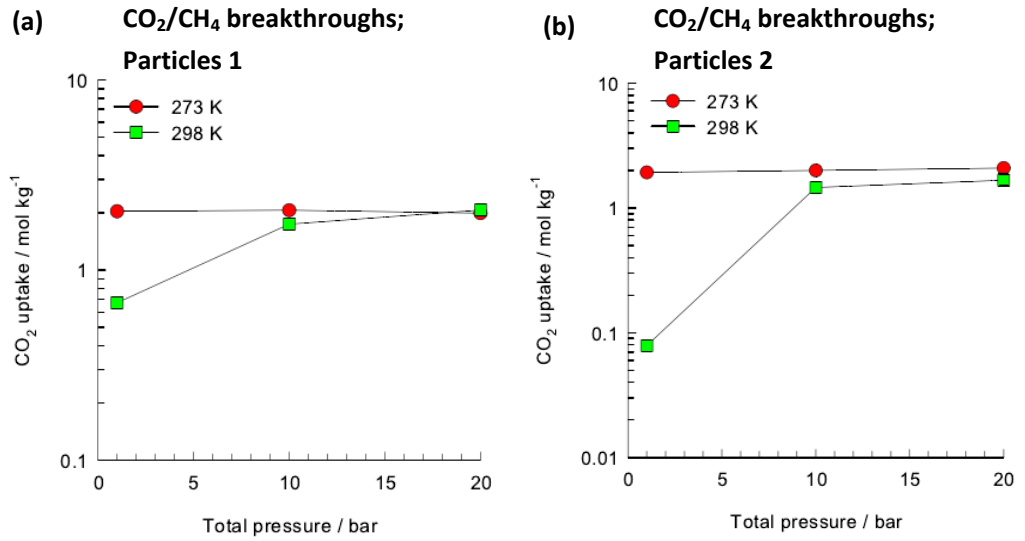

Figure S6. (a, b) CO_2 uptake kg of MOF, calculated from the experimental breakthroughs for CO_2/CH_4 mixtures in packed bed with two particles.

(2) We analyze the experimental breakthroughs for separations of CO_2/CH_4 mixtures in packed bed with two particles. Figure S7 present the data on experimental breakthroughs for 50/50 CH_4/N_2 mixtures in packed bed with two particles. The y-axis represents the mole fractions of N_2 and CH_4 in the exit gas phase. The inlet gas is equimolar, at total pressures of 1 bar, 10, and 20 bar. As indicated for [Cu(dhbc)$_2$(4,4'-bipy)] (particles 1) at 20 bar and 195 K, it is possible to produce N_2 with 90% purity during the time interval between t_1, and t_2. The 90% pure N_2 productivity is calculated from

$$N_2\ productivity\ = \frac{c_t Q_t}{m_{ads}} \int_{t_1}^{t_2} (y_{N2,exit}) dt$$

(3)

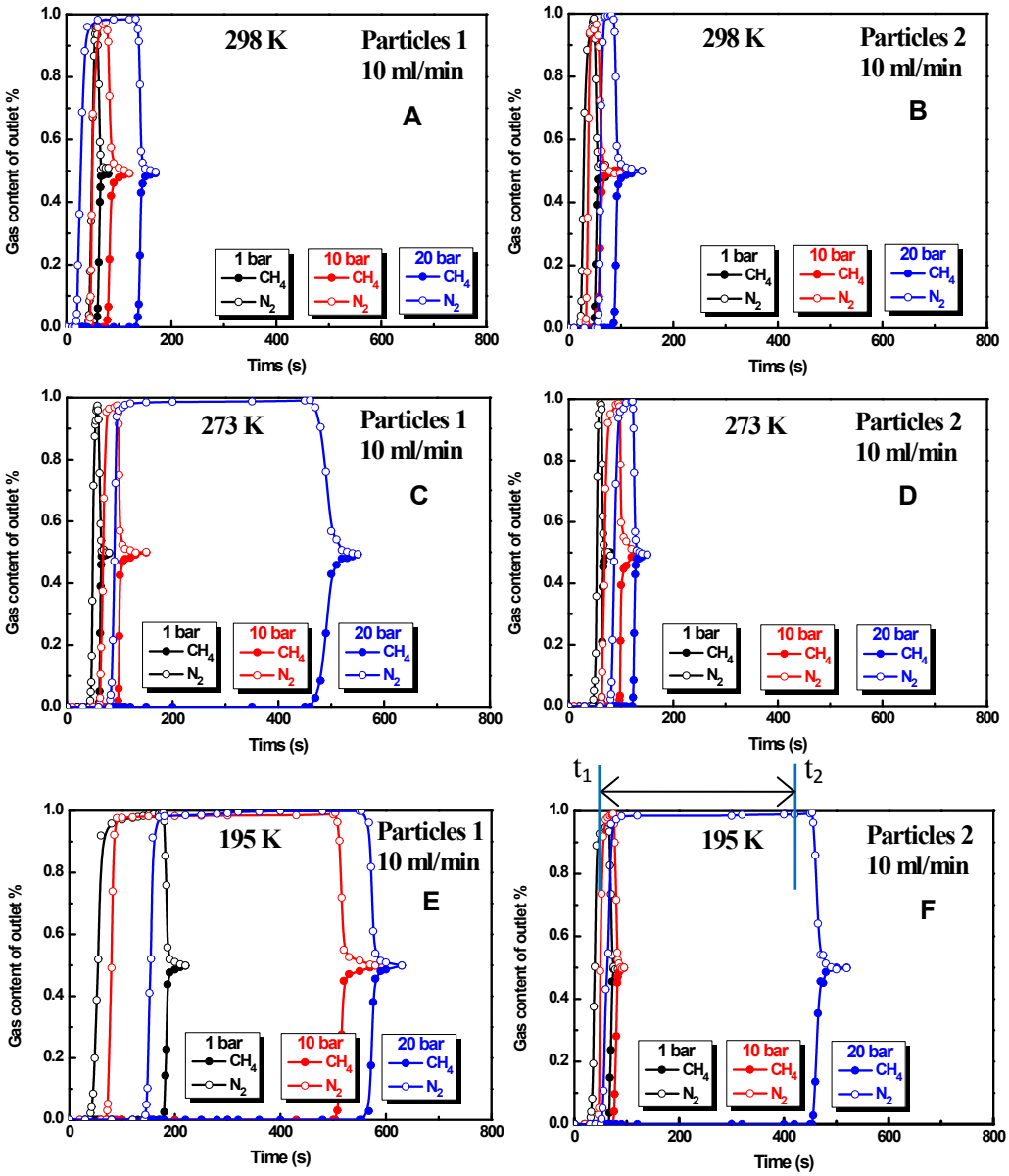

Figure S7. Experimental breakthroughs for 50/50 CH_4/N_2 mixtures in packed bed with[$Cu(dhbc)_2(4,4'\text{-bipy})$] (particles 1) and $Cu(4,4'\text{-bipy})_2(BF_4)_2$ (particles 2). The y-axis represents the mole fractions of N_2 and CH_4 in the exit gas phase. The inlet gas is equimolar, at total pressures of 1 bar, 10, and 20 bar. As indicated for particles 1 at 20 bar and 195 K, it is possible to produce N_2 with 90% purity during the time interval between t_1, and t_2.

Figures S8a, and S8b present plots of the productivity of 90%+ pure N_2 from separation of CH_4/N_2 mixtures with two particles at 195 K, 273 K, and 298 K. The x-axis is the total operating pressure.

The CH_4/N_2 breakthrough curves also allow calculation on the CH_4 uptake from a material balance during the time interval 0 – t_{final}, where t_{final} is the final equilibration time.

$$CH_4\ uptake = \frac{c_t Q_t}{m_{ads}} \int_0^{t_{final}} (y_{CH4,exit} - y_{CH4,exit})dt \quad (4)$$

Figures S9a, and S9b present plots of the CH_4 uptake per kg of MOF, calculated from the experimental breakthroughs in packed bed with [$Cu(dhbc)_2(4,4'\text{-bipy})$] (particles 1) and $Cu(4,4'\text{-bipy})_2(BF_4)_2$ (particles 2).

The productivity of 90%+ pure N_2 correlates with the CH_4 uptake; this is demonstrated in Figure S10.

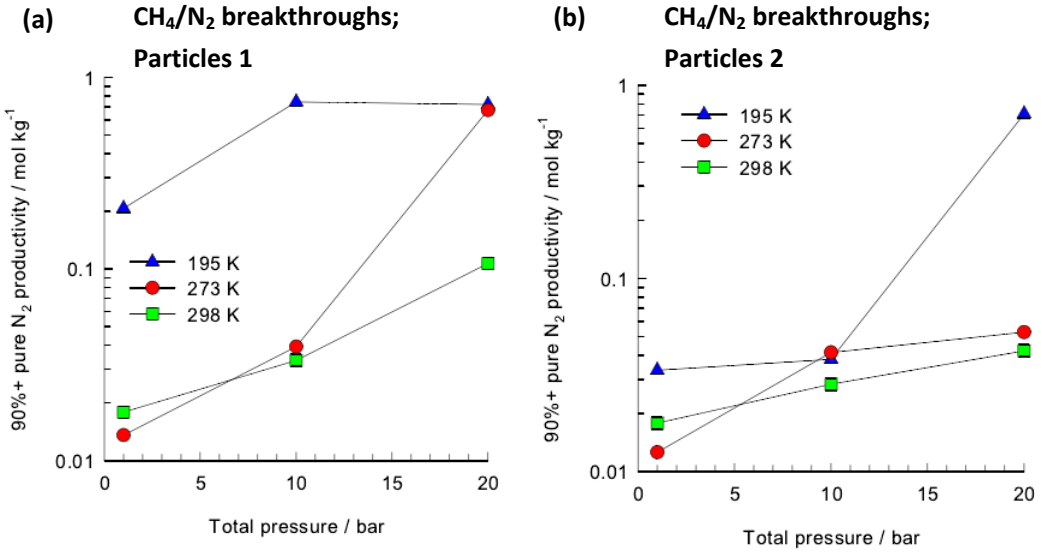

Figure S8. (a, b) Productivity of 90%+ pure N_2 for CH_4/N_2 mixture breakthroughs with two particles at 195 K, 273 K, and 298 K. The x-axis is the total operating pressure.

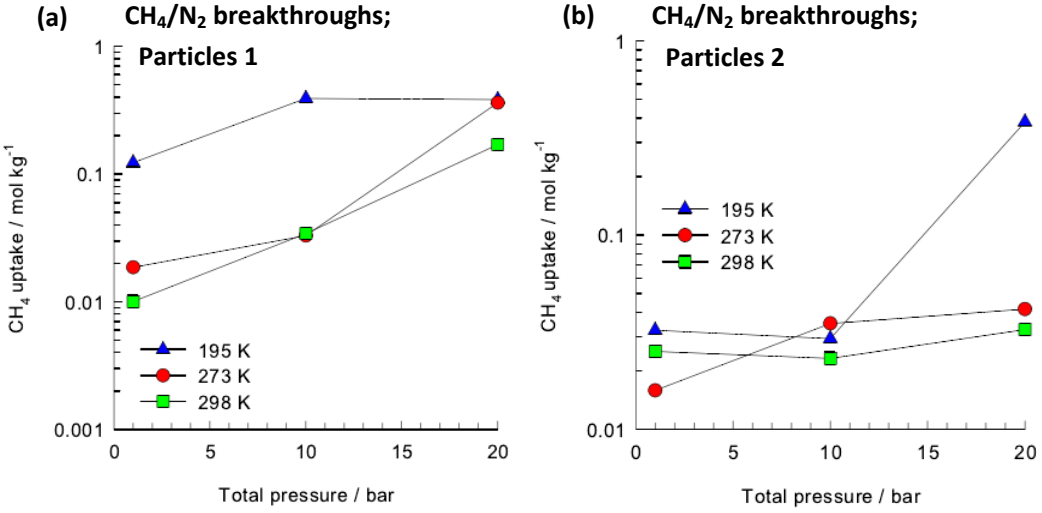

Figure S9. (a, b) CH_4 uptake per kg of MOF, calculated from the experimental breakthroughs in packed bed with two particles. The x-axis is the total operating pressure.

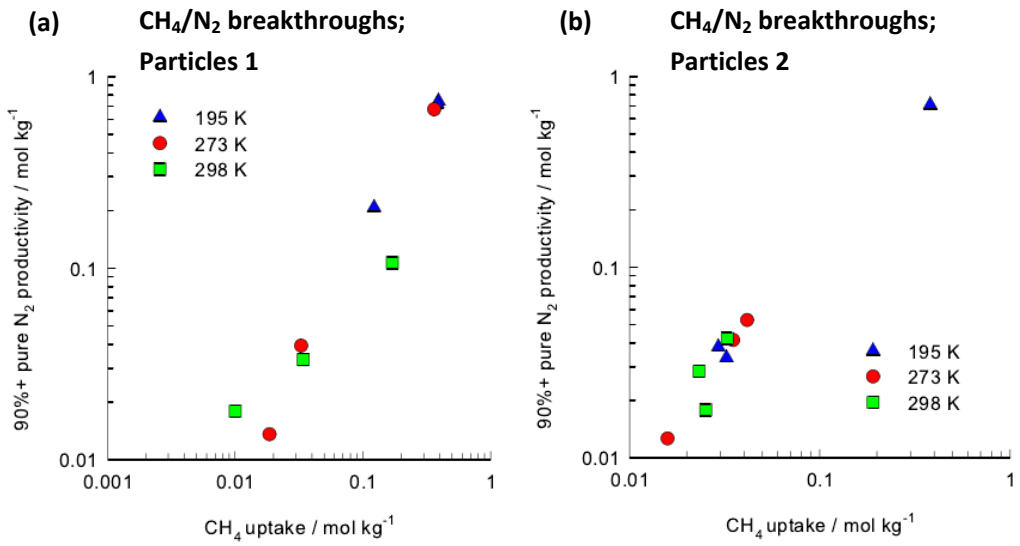

Figure S10. (a, b) Plot of productivity of 90%+ pure N_2 versus the CH_4 uptake in the two flexible MOFs.

Conclusions

The important conclusion that we can be drawn from our breakthrough experiments is that both MOFs possess the capability of separation CO_2/CH_4 of CH_4/N_2 mixtures at pressures ranging to 20 bar, that is of relevance in industry. For each separation it is possible to obtain purified CH_4 and N_2, respectively, with high productivities.

Notation

c_i molar concentration of species *i* in gas mixture, mol m^{-3}

c_{i0} molar concentration of species *i* in gas mixture at inlet to adsorber, mol m^{-3}

c_t total molar concentration of gas mixture, mol m^{-3}

d internal diameter of breakthrough tube, m

L length of packed bed adsorber, m

m_{ads} mass of adsorbent packed into the breakthrough apparatus, kg

p_i partial pressure of species *i* in mixture, Pa

p_t total system pressure, Pa

q_i component molar loading of species *i*, mol kg^{-1}

q_t total molar loading in mixture, mol kg^{-1}

q_{sat} saturation loading, mol kg^{-1}

Q_t total volumetric flow rate, m^3 s^{-1}

t time, s

T absolute temperature, K

V_{ads} volume of adsorbent packed into the breakthrough apparatus, m^3

Subscripts

i referring to component *i*

t referring to total mixture

6. CO_2/CH_4 (50%/50%) separation cycling experiments on two particles at 298 K

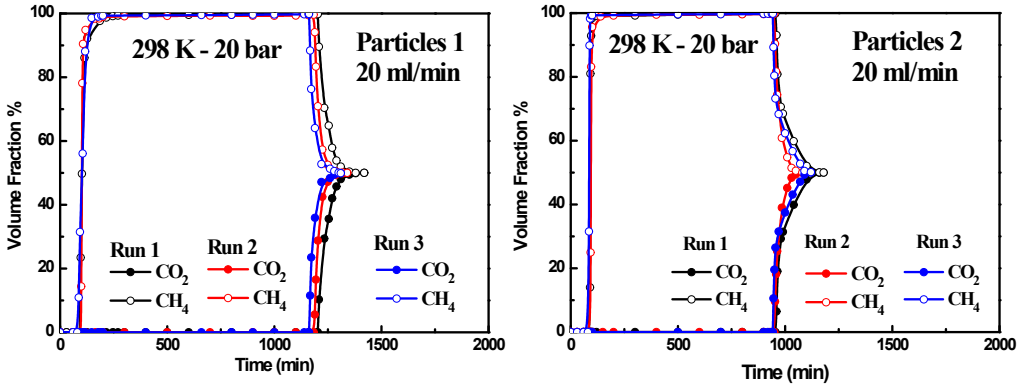

Figure S11. CO_2/CH_4 (50%/50%) separation cycling experiments on two particles at 298 K.

7. Dynamic sorption of CO_2, CH_4, and N_2 on the two flexible MOFs

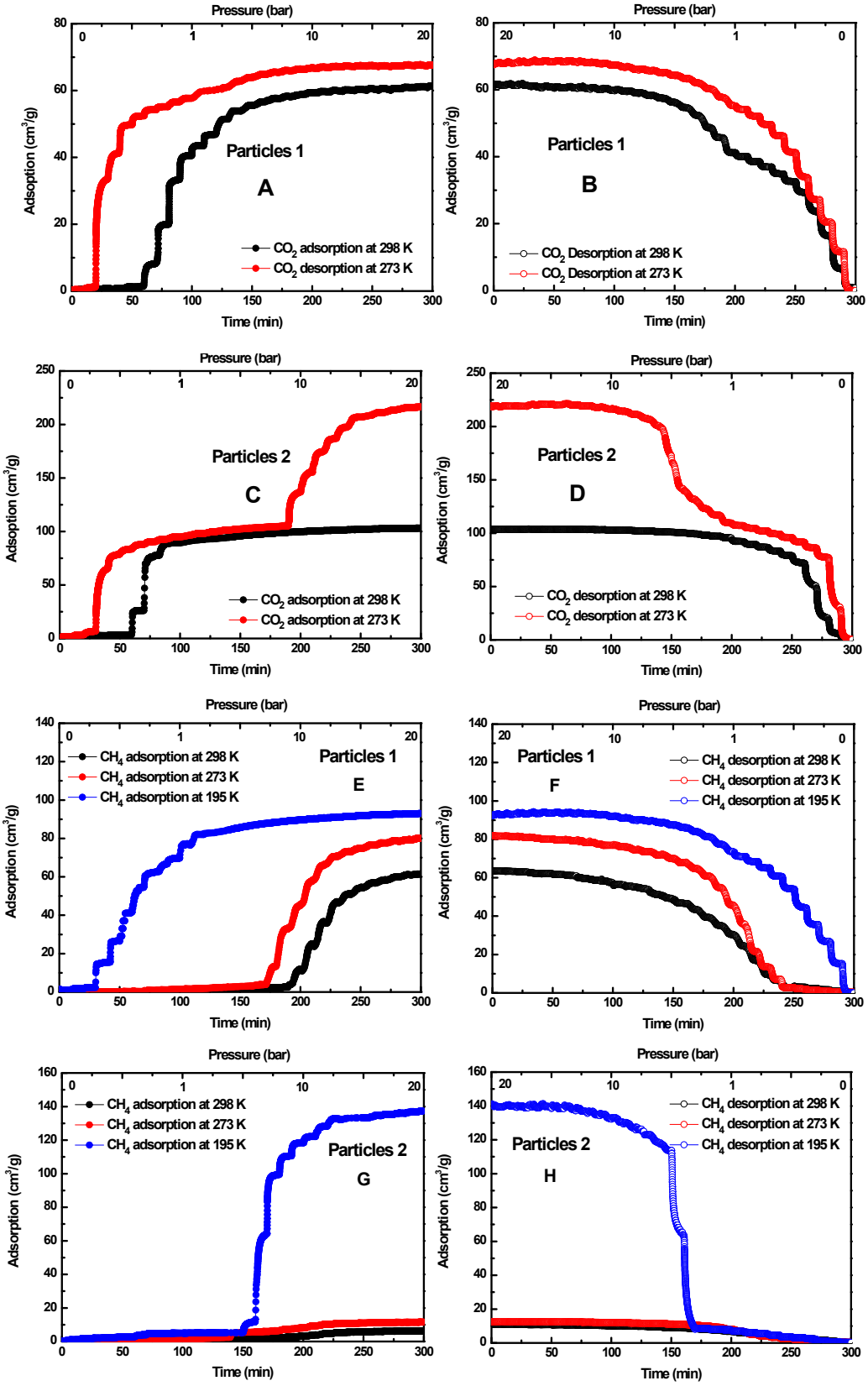

Figure S12. Dynamic CO_2 and CH_4 adsorption (filled) and desorption (opened) isotherms on particles 1 and particles 2 (298 K -195 K).

8. H_2O vapor adsorption on particles 1 and 2 at 298 K with volume and structural changes

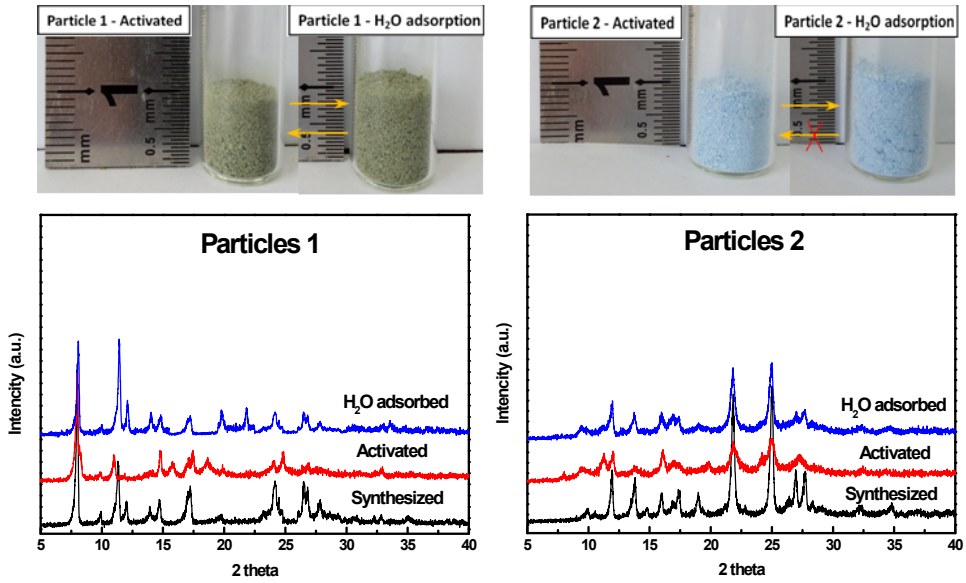

Figure S13. H_2O vapor adsorption on particles 1 and 2 at 298 K with volume and structural changes.

9. Structural stability of two particles heated in air, H_2O, CH_3CH_2OH and H_2O/CH_3CH_2OH

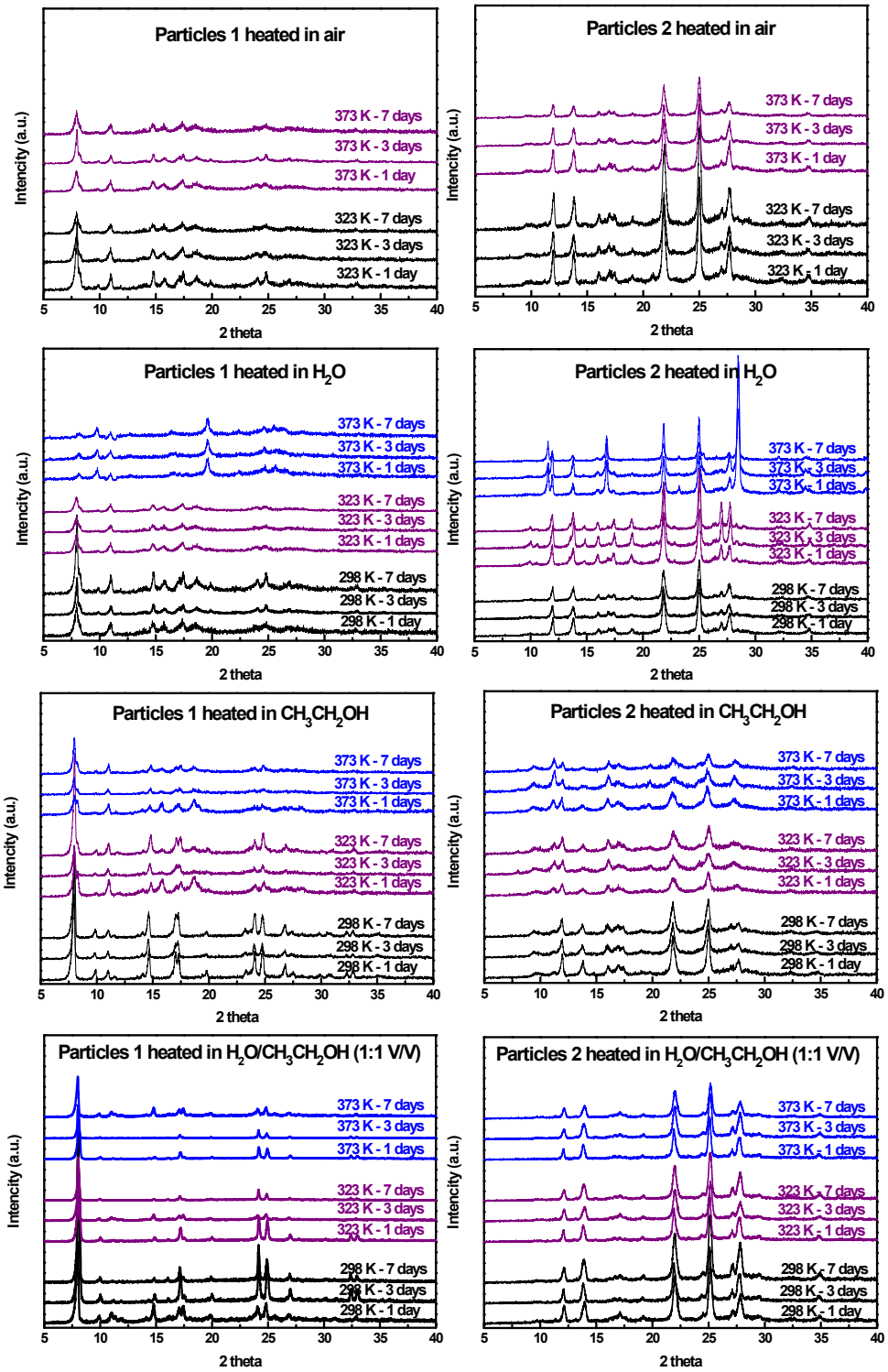

Figure S14. PXRD patterns for particles 1 and 2 heated in air, H_2O, CH_3CH_2OH and H_2O/CH_3CH_2OH (1:1 V/V).

Patterns were taken at day 1, 3, 7 days (bottom to top).

10. Equimolar CO_2/CH_4 and CH_4/N_2 co-adsorption on two flexible MOFs at 273 K

Equimolar CO_2/CH_4 adsorption on $Cu(dhbc)_2(4,4'\text{-bipy})$(A) and $Cu(4,4'\text{-bipy})_2(BF_4)_2$(B) at 273 K

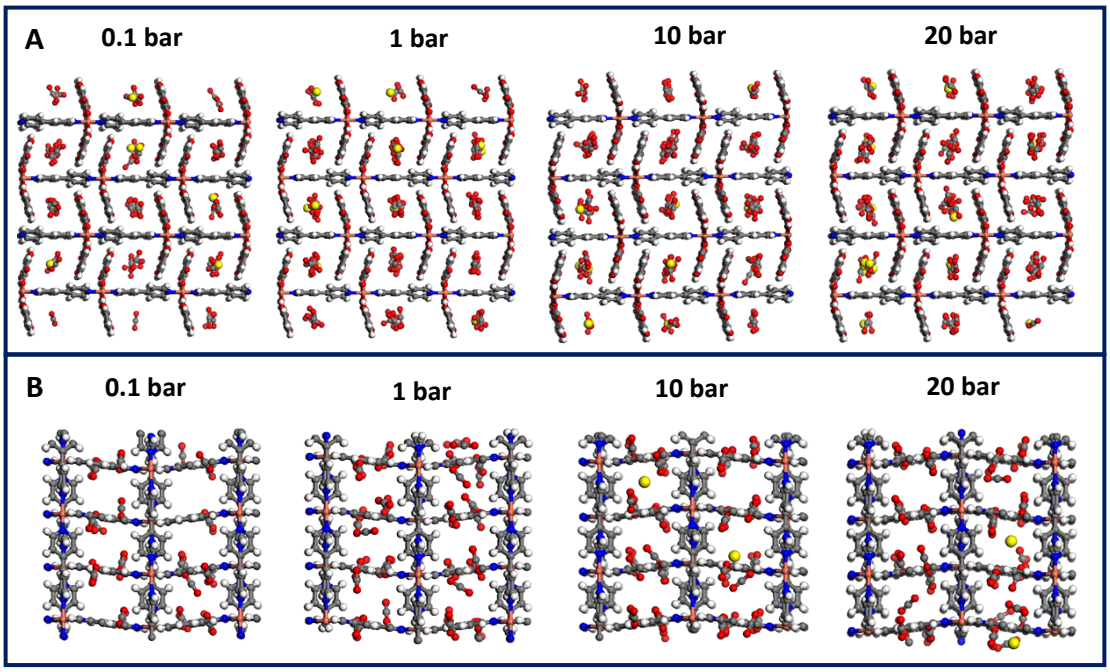

Equimolar CH_4/N_2 adsorption on $Cu(dhbc)_2(4,4'\text{-bipy})$(C) and $Cu(4,4'\text{-bipy})_2(BF_4)_2$(D) at 273 K

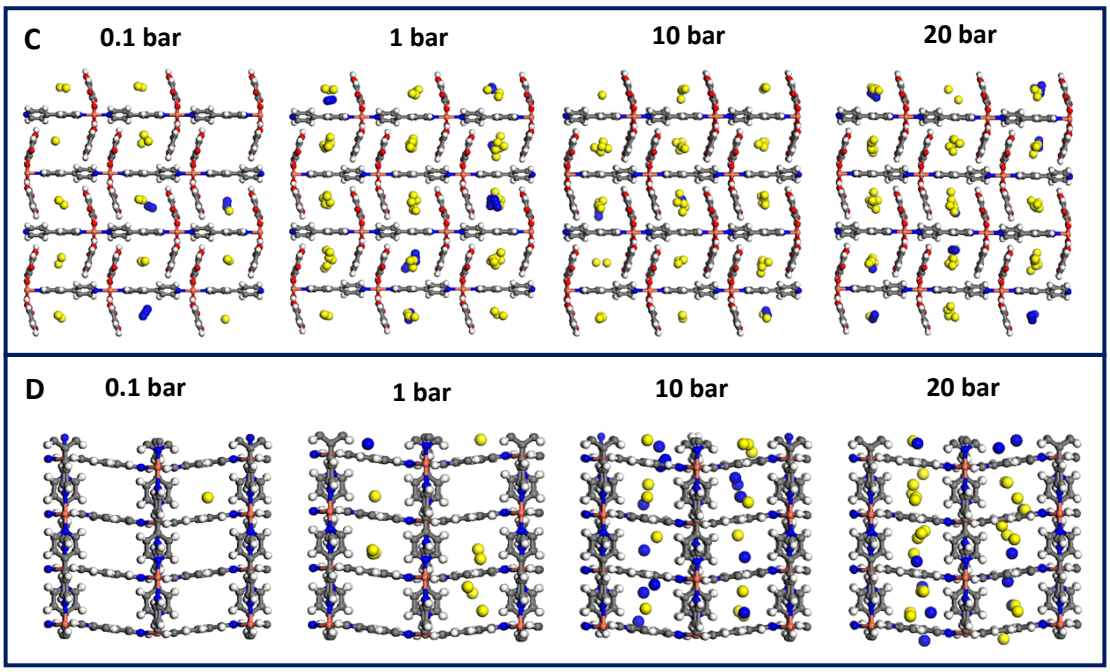

Figure S15. Equimolar CO_2/CH_4 and CH_4/N_2 co-adsorption on $Cu(dhbc)_2(4,4'\text{-bipy})$ and $Cu(4,4'\text{-bipy})_2(BF_4)_2$ simulated by GCMC at 0.1, 1, 10, 20 bar and 273 K.